

Effect of R -site substitution and the pressure on stability of $R\text{Fe}_{12}$: A first-principles study

Yosuke Harashima,^{1,3} Taro Fukazawa,^{1,3} Hiori Kino,^{2,3} and Takashi Miyake^{1,2,3}

¹Research Center for Computational Design of Advanced Functional Materials, National Institute of Advanced Industrial Science and Technology, Tsukuba, Ibaraki 305-8568, Japan

²Center for Materials Research by Information Integration, MaDIS, National Institute for Materials Science, Tsukuba, Ibaraki 305-0047, Japan

³Elements Strategy Initiative Center for Magnetic Materials, National Institute for Materials Science, Tsukuba, Ibaraki 305-0047, Japan

(Dated: 26 September 2018)

We theoretically study the structural stability of $R\text{Fe}_{12}$ with the ThMn_{12} structure (R : rare-earth element, La, Pr, Nd, Sm, Gd, Dy, Ho, Er, Tm, Lu, Y, or Sc, or group-IV element, Zr or Hf) based on density functional theory. The formation energy has a strong correlation with the atomic radius of R . The formation energy relative to simple substances decreases as the atomic radius decreases, except for $R = \text{Sc}$ and Hf, while that relative to $R_2\text{Fe}_{17}$ and bcc Fe has a minimum for $R = \text{Dy}$. The present results are consistent with recent experimental reports in which the partial substitution of Zr at R sites stabilizes $R\text{Fe}_{12}$ -type compounds with $R = \text{Nd}$ or Sm. Our results also suggest that the partial substitution of Y, Dy, Ho, Er, or Tm for Nd or Sm is a possible way to enhance the stability of the ThMn_{12} structure. Under hydrostatic pressure, the formation enthalpy decreases up to ≈ 6 GPa and then starts to increase at higher pressures.

I. INTRODUCTION

The saturation magnetization and magnetocrystalline anisotropy are key quantities that define the performance of a magnet compound. A high content of iron is considered preferable for the former, while rare-earth elements are used as a source of the latter in many cases. From this viewpoint, $R\text{Fe}_{12}$ -type compounds (R : a rare-earth element) with the ThMn_{12} structure have been studied as promising magnet compounds for a long time.^{1–3} $R\text{Fe}_{12}$ contains a higher atomic percentage of Fe (92 at%) than other magnet compounds, e.g., $\text{Nd}_2\text{Fe}_{14}\text{B}$ (82 at%) and $R_2\text{Fe}_{17}$ (89 at%). A quantitative prediction was presented by theoretical work on NdFe_{12}N ⁴ and then confirmed by the experimental realization of NdFe_{12}N by epitaxial growth.⁵ Here, N is introduced to enhance the magnetic properties,^{6,7} and the effects of other typical elements have also been theoretically studied to improve the magnetic properties.^{8,9}

One issue is that $R\text{Fe}_{12}$ is considered to be thermodynamically unstable,¹⁰ and partial substitution for Fe atoms is essential for the stabilization of a bulk system with the ThMn_{12} structure. In the absence of stabilizing elements, $R_2\text{Fe}_{17}$ phases are typically generated instead of $R\text{Fe}_{12}$.^{11,12} Ti is a typical stabilizing element. $\text{SmFe}_{11}\text{Ti}$ ^{13,14} and $\text{NdFe}_{11}\text{TiN}$ ^{6,7} were synthesized around 1990. A disadvantage of the introduction of stabilizing elements is the significant reduction in the saturation magnetization. As a matter of fact, both $\text{SmFe}_{11}\text{Ti}$ and $\text{NdFe}_{11}\text{TiN}$ have an inferior magnetization compared to that of $\text{Nd}_2\text{Fe}_{14}\text{B}$ (e.g., summarized in Table 1 of Ref. 15).

In order to overcome the reduction in the magnetization, a search for another stabilizing element has been conducted. Stabilization by substituting Fe with several

elements (V, Cr, Mn, Mo, W, Al, and Si) have been reported so far,^{13,16–20} but the reduction in the magnetization is still large. It is theoretically suggested that Co can stabilize the ThMn_{12} structure and retain a large magnetic moment.²¹ Though a high magnetization in $\text{Sm}(\text{Fe},\text{Co})_{12}$ films has been experimentally reported recently,²² thermodynamic stabilization by doping with Co has yet to be confirmed.

Recently, $(\text{Nd},\text{Zr})(\text{Fe},\text{Co})_{11.5}\text{Ti}_{0.5}\text{N}_\alpha$ and $(\text{Sm},\text{Zr})(\text{Fe},\text{Co})_{11.5}\text{Ti}_{0.5}$ were synthesized by the strip casting method,^{23–26} which is more practical in industrial applications than the epitaxial growth. Although these compounds contain a smaller amount of Ti than previously synthesized $R\text{Fe}_{12}$ -type compounds without Zr, the ThMn_{12} structure is realized. This suggests that the partial occupation of Zr at the R sites contributes to the stabilization of the ThMn_{12} structure. Therefore, the substitution of R (not Fe sites) is another possible route for stabilizing $R\text{Fe}_{12}$ -type compounds.

In the present work, we theoretically examine a series of R elements— $R = \text{La}, \text{Pr}, \text{Sm}, \text{Gd}, \text{Dy}, \text{Ho}, \text{Er}, \text{Tm}, \text{Lu}, \text{Y}, \text{Sc}, \text{Zr},$ and Hf—as possible stabilizing elements that occupy the rare-earth sites in $R\text{Fe}_{12}$. We calculate the formation energy of $R\text{Fe}_{12}$ relative to (i) simple substances and (ii) $R_2\text{Fe}_{17}$ and bcc Fe based on density functional theory and analyze the R dependence. The obtained results are discussed in connection with experiments on the partial substitution of Zr for $R = \text{Nd}$ or Sm. We then study the effect of the hydrostatic pressure in terms of the stability of $R\text{Fe}_{12}$. This paper is organized as follows. The computational methods are described in Sec. II. The calculated formation energy of $R\text{Fe}_{12}$ and the effect of the hydrostatic pressure are presented in Sec. III. The paper is concluded in Sec. IV.

II. CALCULATION METHODS

We perform first-principles calculations by using QMAS (the Quantum Materials Simulator),²⁷ which is based on density functional theory^{28,29} and the projector augmented-wave method.^{30,31} We use the Perdew–Burke–Ernzerhof (PBE) formula³² in the generalized gradient approximation (GGA) for the exchange-correlation energy functional. We sample $8 \times 8 \times 8$ k points, and the cutoff energy for the plane wave basis is set to 40.0 Ry. The $4f$ electrons of Pr, Nd, Sm, Gd, Dy, Ho, Er, and Tm atoms are treated as spin-polarized open-core states, and those of the Lu atom are treated as core states. The number of occupied $4f$ states is fixed to 2 (Pr), 3 (Nd), 5 (Sm), 7 (Gd), 9 (Dy), 10 (Ho), 11 (Er), 12 (Tm), and 14 (Lu). The electron configuration is determined by Hund’s first rule. For light rare-earth elements (from Pr to Gd), all $4f$ electrons are assumed to be in minority spin states. For heavy rare-earth elements (from Dy to Tm), the minority spin states of the $4f$ orbitals are fully occupied by seven electrons, and the other electrons are in majority spin states. Note that the local spin moment at R is antiparallel to the total spin moment. Spin-orbit coupling is not included in the self-consistent calculation. The reliability of the open-core treatment has been discussed, e.g., in Ref. 33, and we also check the reliability by calculating the formation energy with GGA + U , as shown in Appendix A.

We study $R\text{Fe}_{12}$ with the ThMn_{12} structure for $R = \text{La, Pr, Nd, Sm, Gd, Dy, Ho, Er, Tm, Lu, Y,}$ and Sc —rare-earth elements—and $R = \text{Zr}$ and Hf —group-IV elements. The preferential sites for the group-IV elements are discussed in Appendix B. As reference systems, $R_2\text{Fe}_{17}$ with the $\text{Th}_2\text{Zn}_{17}$ structure, $R_2\text{Fe}_{17}$ with the $\text{Th}_2\text{Ni}_{17}$ structure, and the simple substances of R and Fe are studied. For Fe, the bcc structure is assumed; for $R = \text{La, Pr, Nd,}$ and Sm , the dhcp structure is assumed; and for $R = \text{Gd, Dy, Ho, Er, Tm, Lu, Y, Sc, Zr,}$ and Hf , the hcp structure is assumed. The structures of $R\text{Fe}_{12}$, $R_2\text{Fe}_{17}$, and the simple substances are computationally optimized. The calculation well-reproduces the experimental lattice constants for existing crystals, e.g., $\text{Sm}_2\text{Fe}_{17}$.^{34–36} The calculated lattice constants and the inner coordinates of $R\text{Fe}_{12}$ and $R_2\text{Fe}_{17}$ are shown in Sec. SA of the Supplemental Material.³⁷ From the obtained structures of the simple substances, we deduce the atomic radii (r_R^{calc} and $r_{\text{Fe}}^{\text{calc}}$) of the elements: half of the shortest bond lengths is used as the atomic radii. These values are tabulated in Sec. SB of the Supplemental Material.³⁷

III. RESULTS AND DISCUSSION

We first discuss the values of the energy for forming $R\text{Fe}_{12}$ from the simple substances R and Fe. Let us denote the formation energy of a substance X via the chemical reaction $X' + X'' \rightarrow X$ by $\Delta E |^{X \leftarrow X' + X''}$. Figure 1

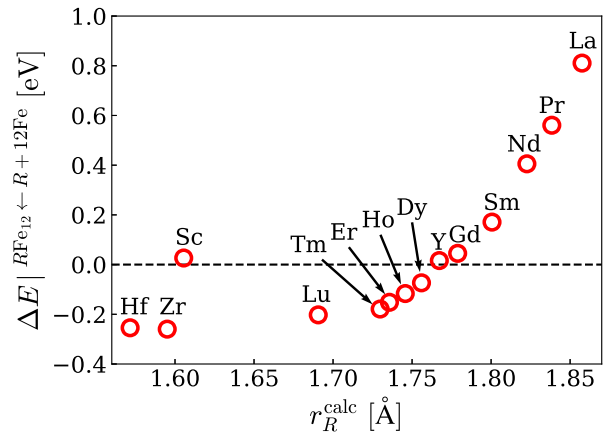


FIG. 1. (Color online) Values of the formation energy $\Delta E |^{R\text{Fe}_{12} \leftarrow R + 12\text{Fe}}$ defined in Eq. (1) for $R = \text{La, Pr, Nd, Sm, Gd, Dy, Ho, Er, Tm, Lu, Y, Sc, Zr,}$ and Hf as a function of the atomic radius r_R^{calc} .

shows the values of $\Delta E |^{R\text{Fe}_{12} \leftarrow R + 12\text{Fe}}$ as a function of r_R^{calc} . This energy is calculated by

$$\Delta E |^{R\text{Fe}_{12} \leftarrow R + 12\text{Fe}} \equiv E[R\text{Fe}_{12}] - (E[R] + 12E[\text{Fe}]), \quad (1)$$

where $E[\cdot]$ denotes the total energy of the system in brackets per formula unit. There is a trend toward a decrease in the formation energy as the calculated atomic radii (r_R^{calc}) decreases. When r_R^{calc} is small, however, this trend does not hold. The value for Sc is exceptionally high. The value for Hf is slightly higher than that for Zr, although Hf has a smaller r_R^{calc} than Zr. Although we do not explicitly show other factors, e.g., the valency, than the atomic size, they may affect the results.

Considering the experimental indication that the $R_2\text{Fe}_{17}$ phase is a competing phase, we also calculate the formation energy of $R\text{Fe}_{12}$ relative to $R_2\text{Fe}_{17}$ and bcc Fe, defined by

$$\begin{aligned} \Delta E |^{R\text{Fe}_{12} \leftarrow \frac{1}{2}R_2\text{Fe}_{17} + \frac{7}{2}\text{Fe}} \\ \equiv E[R\text{Fe}_{12}] - \left(\frac{1}{2}E[R_2\text{Fe}_{17}] + \frac{7}{2}E[\text{Fe}] \right). \end{aligned} \quad (2)$$

We consider two cases for $R_2\text{Fe}_{17}$: one with the (rhombohedral) $\text{Th}_2\text{Zn}_{17}$ structure and the other with the (hexagonal) $\text{Th}_2\text{Ni}_{17}$ structure. The energy difference between the two structures is discussed in Sec. SC of the Supplemental Material.³⁷ Figure 2 shows the values of $\Delta E |^{R\text{Fe}_{12} \leftarrow \frac{1}{2}R_2\text{Fe}_{17} + \frac{7}{2}\text{Fe}}$ for the two cases. The qualitative behavior is insensitive to the choice of structures. As r_R^{calc} decreases to ~ 1.75 Å, $\Delta E |^{R\text{Fe}_{12} \leftarrow \frac{1}{2}R_2\text{Fe}_{17} + \frac{7}{2}\text{Fe}}$ decreases. It has a minimum for $R = \text{Dy}$ and increases as r_R^{calc} decreases further, which is in sharp contrast with the behavior of $\Delta E |^{R\text{Fe}_{12} \leftarrow R + 12\text{Fe}}$. The formation energy is positive even for $R = \text{Dy}$. This indicates that one cannot make the $R\text{Fe}_{12}$ phase more stable than $R_2\text{Fe}_{17}$,

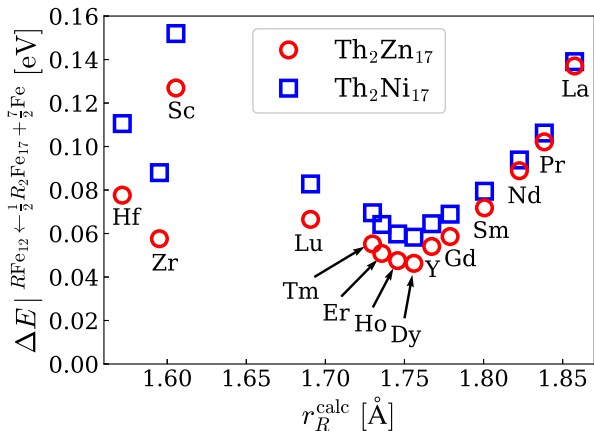


FIG. 2. (Color online) Values of the formation energy $\Delta E |_{R\text{Fe}_{12} \leftarrow \frac{1}{2}R_2\text{Fe}_{17} + \frac{7}{2}\text{Fe}}$ defined in Eq. (2) for $R = \text{La}, \text{Pr}, \text{Nd}, \text{Sm}, \text{Gd}, \text{Dy}, \text{Ho}, \text{Er}, \text{Tm}, \text{Lu}, \text{Y}, \text{Sc}, \text{Zr},$ and Hf as a function of the atomic radius r_R^{calc} . The formation energies relative to $R_2\text{Fe}_{17}$ with the (rhombohedral) $\text{Th}_2\text{Zn}_{17}$ structure and those with the (hexagonal) $\text{Th}_2\text{Ni}_{17}$ structure are shown.

and partial substitution for Fe is necessary for stabilizing the ThMn_{12} structure. However, an appropriate choice of R possibly reduces the necessary amount of stabilizing elements that partially substitute for Fe in synthesizing a material with the ThMn_{12} structure.

As mentioned in Sec. I, $(\text{Nd}, \text{Zr})(\text{Fe}, \text{Co})_{11.5}\text{Ti}_{0.5}\text{N}_\alpha$ and $(\text{Sm}, \text{Zr})(\text{Fe}, \text{Co})_{11.5}\text{Ti}_{0.5}$ have been synthesized.^{23–26} These experiments suggest that the partial substitution of Zr for Nd and Sm enhances the stability of $\text{Nd}(\text{Fe}, \text{Co}, \text{Ti})_{12}\text{N}$ and $\text{Sm}(\text{Fe}, \text{Co}, \text{Ti})_{12}$, respectively. The question is if there is a better element than Zr that contributes to the stabilization of the ThMn_{12} structure. Figure 2 shows that the formation energy (Eq. (2)) is lower for $R = \text{Y}, \text{Dy}, \text{Ho}, \text{Er},$ and Tm than for Zr. We can expect that the partial substitution of these elements for Nd or Sm enhances the stability of the ThMn_{12} structure more than Zr.

The above results imply that the size of R is essential in the stability of $R\text{Fe}_{12}$. Figure 3 shows the lattice constants a and c . The a axis shortens as r_R^{calc} decreases, while the c axis is insensitive to r_R^{calc} . This trend is consistent with the experimental observation that a in $(\text{Nd}, \text{Zr})(\text{Fe}, \text{Co})_{11.5}\text{Ti}_{0.5}\text{N}_\alpha$ decreases with increasing Zr concentration, whereas c is insensitive to the Zr concentration.^{24,26}

These results motivate us to consider a possibility that applied pressure stabilizes $R\text{Fe}_{12}$. To discuss the stability under hydrostatic pressure, we estimate the formation enthalpy defined as follows:

$$\Delta H(p) \equiv H[R\text{Fe}_{12}](p) - \left(\frac{1}{2}H[R_2\text{Fe}_{17}](p) + \frac{7}{2}H[\text{Fe}](p) \right), \quad (3)$$

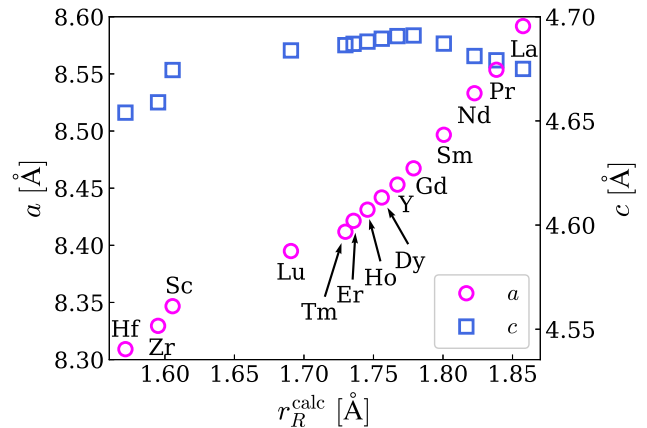


FIG. 3. (Color online) Lattice constants a and c of $R\text{Fe}_{12}$ obtained by structural optimization for $R = \text{La}, \text{Pr}, \text{Nd}, \text{Sm}, \text{Gd}, \text{Dy}, \text{Ho}, \text{Er}, \text{Tm}, \text{Lu}, \text{Y}, \text{Sc}, \text{Zr},$ and Hf as a function of the atomic radius r_R^{calc} . The left (a) and right (c) scales are taken so that the value corresponding to a vertical distance along the right axis becomes the value along the left axis multiplied by c/a for $R = \text{Nd}$.

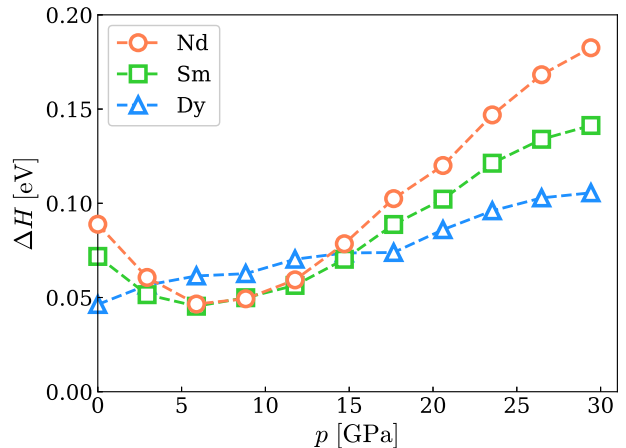


FIG. 4. (Color online) Formation enthalpy defined by Eq. (3) as a function of the pressure p . The orange circles denote values for $R = \text{Nd}$, the green squares are for $R = \text{Sm}$, and the blue triangles denote values for $R = \text{Dy}$.

where $H[\cdot](p)$ denotes the enthalpy of the system in brackets under pressure p . At $p = 0$, $\Delta H(0)$ is equivalent to $\Delta E |_{R\text{Fe}_{12} \leftarrow \frac{1}{2}R_2\text{Fe}_{17} + \frac{7}{2}\text{Fe}}$. We perform computational optimization of the structure of $R\text{Fe}_{12}$, $R_2\text{Fe}_{17}$ with the rhombohedral $\text{Th}_2\text{Zn}_{17}$ structure, and bcc Fe under hydrostatic pressure. The applied pressure shrinks NdFe_{12} anisotropically (see Sec. SE of the Supplemental Material³⁷). Its a axis is shortened more than the c axis. The tendency of a to be more susceptible than c was seen also in their dependence on the atomic radius of R , as seen in Fig. 3. The a axis becomes similar to that of DyFe_{12}

at $p \approx 4$ GPa, and it becomes similar to that of ZrFe_{12} at $p \approx 10$ GPa. The formation enthalpy as a function of the pressure for $R = \text{Nd}$ and Sm is shown in Fig. 4. As the pressure increases, the values of ΔH decrease up to $p \approx 6$ GPa and then start to increase when the pressure increases further. Although applying a pressure cannot lead to a negative enthalpy, it is expected that amount of stabilizing elements for Fe, such as Ti, can be reduced by synthesis under a hydrostatic pressure of ≈ 6 GPa. Admittedly, the pressure is too high to be applied in an industrial production process, the pressure is experimentally applicable and it may offer useful information in a viewpoint of stabilization by controlling the lattice. We confirmed that further reduction cannot be obtained in the case of $R = \text{Dy}$ as shown in Fig. 4.

The qualitative difference in the pressure dependencies shown in Fig. 4 can be explained as follows. Because we are considering a temperature of zero, the enthalpy under a finite pressure $H(p)$ is written as

$$H(p) = H(0) + \int_0^p dp' V(p') \quad (4)$$

$$= H(0) + V(0)p - \frac{K}{2}p^2 + \dots, \quad (5)$$

where $V(p)$ is the volume of the system under the pressure p and K is a coefficient that is related to the bulk modulus, B_0 , by $K \equiv -dV/dp|_{p=0} = V(0)/B_0$. In the first order of p , the increase in the enthalpy is proportional to the volume at zero pressure. It follows from the second-order term of p that a phase is more easily stabilized by pressure when it is softer. This can be expressed in a more general form by noting that the higher-order terms are written as $\int_0^p dp' (V(p') - V(0))$. This is a general expression of “softness” because it refers to the volume change under a given pressure p .

At a pressure of zero, the gradient of $\Delta H(p)$ in Eq. (3) is determined by a difference in the volume at a pressure of zero, ΔV_0 .

$$\Delta V_0 \equiv V[\text{RFe}_{12}](0) - \left(\frac{1}{2}V[\text{R}_2\text{Fe}_{17}](0) + \frac{7}{2}V[\text{Fe}](0) \right). \quad (6)$$

$V[\cdot](0)$ denotes the volume of the system in brackets per formula unit at $p = 0$. The values of ΔV_0 are -1.7 \AA^3 for Nd, -1.4 \AA^3 for Sm, and 0.4 \AA^3 for Dy, respectively. This is consistent with the behavior of ΔH at a low pressure shown in Fig. 4.

In the second-order approximation, $\Delta H(p)$ in Eq. (3) can be written as

$$\Delta H(p) = \Delta H_0 + \Delta V_0 p - \frac{\Delta K}{2} p^2 \quad (7)$$

$$= -\frac{\Delta K}{2} \left(p - \frac{\Delta V_0}{\Delta K} \right)^2 + \Delta H_0 + \frac{\Delta V_0^2}{2\Delta K}, \quad (8)$$

where

$$\Delta H_0 \equiv H[\text{RFe}_{12}](0) - \left(\frac{1}{2}H[\text{R}_2\text{Fe}_{17}](0) + \frac{7}{2}H[\text{Fe}](0) \right), \quad (9)$$

$$\Delta K \equiv K[\text{RFe}_{12}] - \left(\frac{1}{2}K[\text{R}_2\text{Fe}_{17}] + \frac{7}{2}K[\text{Fe}] \right). \quad (10)$$

$K[\cdot]$ denotes the coefficient $V(0)/B_0$ of the system.

Within the second-order approximation, the minimum of $\Delta H(p)$ always exists at $p > 0$ when $\Delta V_0 < 0$ and $\Delta K < 0$ hold, or more intuitively, when RFe_{12} is smaller and harder than R_2Fe_{17} at a temperature of zero. The values estimated from our first-principles calculations are $\Delta K = -0.070 \text{ \AA}^3/\text{GPa}$ and $\Delta V_0 = -1.7 \text{ \AA}^3$ for Nd. These values enable us to predict the existence of the dip from the information at a pressure of zero. Note that, however, Eq. (8) well-describes the behavior of the curves in Fig. 4 only for small pressures. The valid range does not cover the argument of the minimum $\Delta H(p)$, $\Delta V_0/\Delta K \approx 24 \text{ GPa}$. The higher-order terms omitted in Eq. (7) take effect under high pressure and change the minimum of $\Delta H(p)$ from 24 GPa to 6 GPa.

IV. CONCLUSION

We have performed first-principles calculations of RFe_{12} , where $R = \text{La}, \text{Pr}, \text{Nd}, \text{Sm}, \text{Gd}, \text{Dy}, \text{Ho}, \text{Er}, \text{Tm}, \text{Lu}, \text{Y}, \text{Sc}, \text{Zr},$ and Hf are considered. The formation energy relative to simple substances becomes lower as the atomic radius of R becomes smaller, except for $R = \text{Sc}$ and Hf . The stability of RFe_{12} relative to the R_2Fe_{17} phase was also discussed. We found that ZrFe_{12} has a lower formation energy than NdFe_{12} and SmFe_{12} . This is consistent with the experimental results for the synthesis of $(\text{Nd}, \text{Zr})(\text{Fe}, \text{Co})_{11.5}\text{Ti}_{0.5}\text{N}_\alpha$ and $(\text{Sm}, \text{Zr})(\text{Fe}, \text{Co})_{11.5}\text{Ti}_{0.5}$. We also found that Y, Dy, Ho, Er, and Tm are possible candidates for enhancing the stability of Nd- or Sm- based RFe_{12} -type compounds. The effect of hydrostatic pressure was also discussed in terms of the stability of the NdFe_{12} , SmFe_{12} , and DyFe_{12} phases. In the cases for NdFe_{12} and SmFe_{12} , a hydrostatic pressure of ≈ 6 GPa was found to contribute to the stability of the phases, although the formation enthalpy is still positive.

ACKNOWLEDGMENTS

The authors would like to thank Kiyoyuki Terakura, Shoji Ishibashi, Satoshi Hirose and Hisazumi Akai for fruitful discussions. This work was supported by the Elements Strategy Initiative Project under the auspices of MEXT, by the “Materials research by Information Integration” Initiative (MI²I) project of the Support Program for Starting Up Innovation Hub from the Japan Science and Technology Agency (JST), and also by

MEXT as a social and scientific priority issue (Creation of new functional Devices and high-performance Materials to Support next-generation Industries; CDMSI) to be tackled by using a post-K computer. Computations were partly carried out using the facilities of the Supercomputer Center, the Institute for Solid State Physics, the University of Tokyo, and the supercomputer of ACCMS, Kyoto University and the K computer provided by the RIKEN Advanced Institute for Computational Science (Project IDs:hp150014, hp160227, hp170100, and hp170269).

Appendix A: Comparison between GGA + open-core and GGA + U

TABLE I. Formation energies defined by Eqs. (1) and (2) for NdFe_{12} and rhombohedral $\text{Nd}_2\text{Fe}_{17}$. The value of U is set as 5 eV. The energies are presented in electronvolts.

	Eq. (1)	Eq. (2)
GGA + open-core	0.405	0.084
GGA + U	0.395	0.105

In this appendix, we discuss the reliability of the open-core treatment for $4f$ electrons by comparison with the calculation with the GGA + U method. We calculate the total energy of NdFe_{12} and rhombohedral $\text{Nd}_2\text{Fe}_{17}$ with the GGA + U method. The crystal structures are optimized within the scheme. We use 5 eV as a value of U for the Nd $4f$ orbitals. Table I presents the formation energies calculated with Eqs. (1) and (2). The formation energy calculated with the GGA + open-core treatment agrees with the value calculated with the GGA + U .

Appendix B: Substitution of group-IV elements (Zr, Ti, and Hf)

In order to investigate the site preference of group-IV elements $Z = \text{Ti}, \text{Zr},$ and Hf for the substitution in NdFe_{12} , we calculate $Z\text{Fe}_{12}$ ($2a$ substitution) and $\text{NdFe}_{11}Z$ ($8f, 8i,$ and $8j$ substitution) with structure optimization. Then, we calculate their formation energies from the simple Fe, Nd, and Z phases. In the case of $2a$ substitution, we consider the formation energy of $Z\text{Fe}_{12}$ plus the simple Nd phase from the simple Fe, Nd, and Z phases:

$$\Delta E |^{Z\text{Fe}_{12}+\text{Nd}\leftarrow\text{Nd}+Z+12\text{Fe}} = \Delta E |^{Z\text{Fe}_{12}\leftarrow Z+12\text{Fe}}. \quad (\text{B1})$$

In the other cases, we consider the formation energy of $\text{NdFe}_{11}Z$ plus the simple Fe phase from the simple Fe,

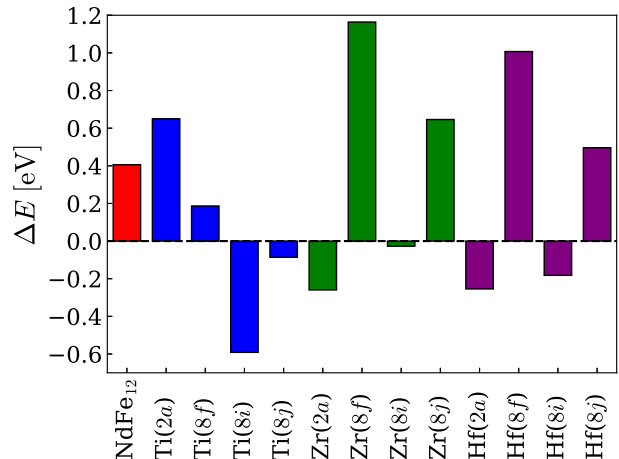


FIG. 5. (Color online) Values of the formation energy for NdFe_{12} , $Z\text{Fe}_{12}$ ($2a$ substitution), and $\text{NdFe}_{11}Z$ ($8f, 8i,$ and $8j$ substitution) defined by Eqs. (B1) and (B2) for $Z = \text{Ti}, \text{Zr},$ and Hf . The labels along the horizontal axis except “ NdFe_{12} ” denote the substituting element and the site of the substitution. The label $\text{Zr}(2a)$, for example, corresponds to ZrFe_{12} and $\text{Ti}(8i)$ to $\text{NdFe}_{11}\text{Ti}$ with one of the $\text{Fe}(8i)$ sites replaced by Ti .

Nd, and Z phases:

$$\Delta E |^{\text{NdFe}_{11}Z+\text{Fe}\leftarrow\text{Nd}+Z+12\text{Fe}} = \Delta E |^{\text{NdFe}_{11}Z\leftarrow\text{Nd}+Z+11\text{Fe}}. \quad (\text{B2})$$

Therefore, we nominally use the common reference system ($\text{Nd}+Z+12\text{Fe}$) to the cases.

The results are shown in Fig. 5. $\text{Ti}(8i)$, $\text{Zr}(2a)$, and $\text{Hf}(2a)$ are the preferential sites for substitution. As for Hf , the $8i$ site is as stable as the $2a$ site. The values of ΔE for the substituted systems are much smaller than that for NdFe_{12} . Therefore, those elements can work positively for the stabilization of the ThMn_{12} phase.

We also evaluate the magnetic moments and magnetizations of the systems considered. Figure 6 shows the magnetic moment m [$\mu_{\text{B}}/\text{f.u.}$] and magnetization $\mu_0 M$ [T], where μ_0 is the vacuum permeability. The magnetization is estimated from the calculated magnetic moment m , volume V , and Bohr magneton μ_{B} by $\mu_0 M = \mu_{\text{B}} m/V$. The values denoted by the open symbols include the value of $g_J J = 3.273 \mu_{\text{B}}$ as the contribution from the Nd $4f$ electrons [g_J : Lande g-factor; J : total angular momentum of the Nd $4f$ electrons]. The values denoted by the filled symbols do not include this contribution.

The magnetic moment m (circle) for $Z\text{Fe}_{12}$ [denoted by $Z(2a)$] in the figure is much less than that for NdFe_{12} . Though it mainly originates from the lack of a Nd $4f$ moment, the differences are larger than $g_J J$ of Nd, which can be seen from the difference between the red open circle and the red filled circle. The magnetizations $\mu_0 M$ are also reduced by Z substitution, as seen from the magnetic moment, but the amounts of reduction in the magnetizations are close to the contribution from the Nd $4f$

moment. This is because Z substitution shrinks the volume, and this shrinkage cancels some of the reduction. Eventually, the reduction in the magnetization falls close to the Nd $4f$ moment.

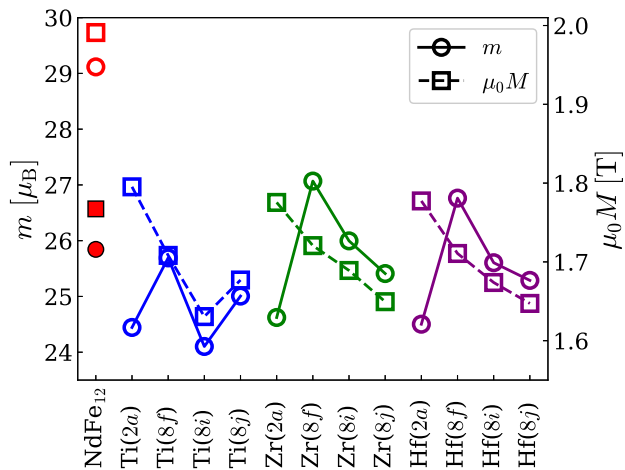


FIG. 6. (Color online) Total magnetic moment [μ_B /f.u.] (open circles) and magnetization [T] (open squares) for NdFe_{12} , $Z\text{Fe}_{12}$, and $\text{NdFe}_{11}Z$ ($Z = \text{Ti}, \text{Zr}$, and Hf). The horizontal labels denote the same systems as in Fig. 5. The red filled circle and square denote the values for NdFe_{12} without the Nd $4f$ moment.

For the substitution of Ti for the Fe sites ($8f$, $8i$, and $8j$), the magnetic moment is drastically reduced, which can be explained by Friedel's concept of a virtual bound state.^{4,38,39} As for $\text{NdFe}_{11}\text{Zr}$ and $\text{NdFe}_{11}\text{Hf}$, the reduction in m is moderate. However, the reduction in terms of the magnetization, μ_0M , is significantly large owing to the volume expansion caused by the introduction of Zr and Hf.

¹K. H. J. Buschow, *J. Magn. Magn. Mater.* **100**, 79 (1991).
²Y. Hirayama, T. Miyake, and K. Hono, *JOM* **67**, 1344 (2015).
³T. Miyake and H. Akai, *J. Phys. Soc. Jpn.* **87**, 041009 (2018).
⁴T. Miyake, K. Terakura, Y. Harashima, H. Kino, and S. Ishibashi, *J. Phys. Soc. Jpn.* **83**, 043702 (2014).
⁵Y. Hirayama, Y. K. Takahashi, S. Hirosawa, and K. Hono, *Scr. Mater.* **95**, 70 (2015).
⁶Y. C. Yang, X. D. Zhang, L. S. Kong, Q. Pan, and S. L. Ge, *Solid State Commun.* **78**, 317 (1991).
⁷Y. C. Yang, X. D. Zhang, S. L. Ge, Q. Pan, L. S. Kong, H. Li, J. L. Yang, B. S. Zhang, Y. F. Ding, and C. T. Ye, *J. Appl. Phys.* **70**, 6001 (1991).

⁸Y. Harashima, K. Terakura, H. Kino, S. Ishibashi, and T. Miyake, *Phys. Rev. B* **92**, 184426 (2015).
⁹T. Fukazawa, H. Akai, Y. Harashima, and T. Miyake, *J. Appl. Phys.* **122**, 053901 (2017).
¹⁰R. Coehoorn, *Phys. Rev. B* **41**, 11790 (1990).
¹¹A. Margarian, J. B. Dunlop, R. K. Day, and W. Kalceff, *J. Appl. Phys.* **76**, 6153 (1994).
¹²H. Suzuki, *AIP Adv.* **7**, 056208 (2017).
¹³K. Ohashi, Y. Tawara, R. Osugi, J. Sakurai, and Y. Komura, *J. Less-Common Met.* **139**, L1 (1988).
¹⁴K. Ohashi, Y. Tawara, R. Osugi, and M. Shima, *J. Appl. Phys.* **64**, 5714 (1988).
¹⁵S. Hirosawa, M. Nishino, and S. Miyashita, *Adv. Nat. Sci.: Nanosci. Nanotechnol.* **8**, 013002 (2017).
¹⁶I. Felner, *J. Less-Common Met.* **72**, 241 (1980).
¹⁷Y. C. Yang, B. Kebe, W. J. James, J. Deportes, and W. Yelon, *J. Appl. Phys.* **52**, 2077 (1981).
¹⁸D. B. D. Mooij and K. H. J. Buschow, *J. Less-Common Met.* **136**, 207 (1988).
¹⁹A. Müller, *J. Appl. Phys.* **64**, 249 (1988).
²⁰X. Z. Wang, B. Chevalier, T. Berlureau, J. Etourneau, J. M. D. Coey, and J. M. Cadogan, *J. Less-Common Met.* **138**, 235 (1988).
²¹Y. Harashima, K. Terakura, H. Kino, S. Ishibashi, and T. Miyake, *J. Appl. Phys.* **120**, 203904 (2016).
²²Y. Hirayama, Y. K. Takahashi, S. Hirosawa, and K. Hono, *Scr. Mater.* **138**, 62 (2017).
²³S. Suzuki, T. Kuno, K. Urushibata, K. Kobayashi, N. Sakuma, K. Washio, H. Kishimoto, A. Kato, and A. Manabe, *AIP Adv.* **4**, 117131 (2014).
²⁴N. Sakuma, S. Suzuki, T. Kuno, K. Urushibata, K. Kobayashi, M. Yano, A. Kato, and A. Manabe, *AIP Adv.* **6**, 056023 (2016).
²⁵T. Kuno, S. Suzuki, K. Urushibata, K. Kobayashi, N. Sakuma, M. Yano, A. Kato, and A. Manabe, *AIP Adv.* **6**, 025221 (2016).
²⁶S. Suzuki, T. Kuno, K. Urushibata, K. Kobayashi, N. Sakuma, K. Washio, M. Yano, A. Kato, and A. Manabe, *J. Magn. Magn. Mater.* **401**, 259 (2016).
²⁷<http://qmas.jp/>.
²⁸P. Hohenberg and W. Kohn, *Phys. Rev.* **136**, B864 (1964).
²⁹W. Kohn and L. J. Sham, *Phys. Rev.* **140**, A1133 (1965).
³⁰P. E. Blöchl, *Phys. Rev. B* **50**, 17953 (1994).
³¹G. Kresse and D. Joubert, *Phys. Rev. B* **59**, 1758 (1999).
³²J. P. Perdew, K. Burke, and M. Ernzerhof, *Phys. Rev. Lett.* **77**, 3865 (1996).
³³Y. Tatetsu, Y. Harashima, T. Miyake, and Y. Gohda, *Phys. Rev. Materials* **2**, 074410 (2018).
³⁴J. M. D. Coey and H. Sun, *J. Magn. Magn. Mater.* **87**, L251 (1990).
³⁵K. Koyama and H. Fujii, *Phys. Rev. B* **61**, 9475 (2000).
³⁶Y. Hirayama, A. K. Panda, T. Ohkubo, and K. Hono, *Scr. Mater.* **120**, 27 (2016).
³⁷See Supplemental Material for (SA) the lattice constants of $R\text{Fe}_{12}$ and $R_2\text{Fe}_{17}$, (SB) the calculated atomic radii of R and Fe, (SC) the difference in the total energies of rhombohedral and hexagonal $R_2\text{Fe}_{17}$, (SD) the bond lengths in $R\text{Fe}_{12}$, and (SE) the lattice distortion in NdFe_{12} and $\text{Nd}_2\text{Fe}_{17}$ induced by hydrostatic pressure.
³⁸J. Friedel, *Il Nuovo Cimento* (1955-1965) **7**, 287 (1958).
³⁹R. Verhoef, F. R. de Boer, Z. Zhi-dong, and K. H. J. Buschow, *J. Magn. Magn. Mater.* **75**, 319 (1988).